



## OPEN ACCESS

### EDITED BY

Izzet Sakalli,  
Eastern Mediterranean  
University, Türkiye

### REVIEWED BY

Yuqiang Li,  
University of Chinese Academy of  
Sciences, China  
Anivid Pedros-Faura,  
University of Colorado Boulder,  
United States

### \*CORRESPONDENCE

Yilong Han,  
✉ hanyl@sdust.edu.cn  
Shanhong Liu,  
✉ shliu\_ast@163.com

RECEIVED 11 December 2025

REVISED 17 March 2026

ACCEPTED 19 March 2026

PUBLISHED 02 April 2026

### CITATION

Feng S, Han Y, Liu S, Tang K and Yan J  
(2026) Numerical integration and  
analysis of mars orbital dynamics.  
*Front. Astron. Space Sci.* 13:1765279.  
doi: 10.3389/fspas.2026.1765279

### COPYRIGHT

© 2026 Feng, Han, Liu, Tang and Yan.  
This is an open-access article  
distributed under the terms of the  
[Creative Commons Attribution License  
\(CC BY\)](https://creativecommons.org/licenses/by/4.0/). The use, distribution or  
reproduction in other forums is  
permitted, provided the original  
author(s) and the copyright owner(s) are  
credited and that the original  
publication in this journal is cited, in  
accordance with accepted academic  
practice. No use, distribution or  
reproduction is permitted which does  
not comply with these terms.

# Numerical integration and analysis of mars orbital dynamics

Shuhao Feng<sup>1</sup>, Yilong Han<sup>1\*</sup>, Shanhong Liu<sup>2,3\*</sup>, Kai Tang<sup>4</sup> and  
Jianguo Yan<sup>5</sup>

<sup>1</sup>College of Geodesy and Geomatics, Shandong University of Science and Technology, Qingdao, China, <sup>2</sup>Intelligent Game and Decision Laboratory, Beijing, China, <sup>3</sup>Defense Innovation Institute, Chinese Academy of Military Science, Beijing, China, <sup>4</sup>Shanghai Astronomical Observatory, Chinese Academy of Sciences, Shanghai, China, <sup>5</sup>State Key Laboratory of Information Engineering in Surveying, Mapping and Remote Sensing, Wuhan University, Wuhan, China

**Introduction:** The high-precision numerical ephemeris of Mars is important for its mission planning, spacecraft navigation, and solar system dynamics studies.

**Methods:** This study systematically compares the dynamical models employed in the DE441, EPM2021, INPOP21a, and PETREL19 ephemerides and evaluates the contributions of the principal perturbation forces to Mars orbit.

**Results:** Over a 30-year integration span, the effects of solar oblateness and the Lense-Thirring relativistic precession lead to the orbital difference on the order of hundreds of meters. Modeling the main asteroid belt as discrete point masses introduces deviations of about tens of kilometers, whereas the ring approximation of the main belt and the model for the Kuiper belt both contribute perturbations on the order of tens of meters. When Mars Express (MEX) ranging, ground-based radar, and VLBI data are combined and weighted based on their average precision, the RMS of orbital differences with respect to JPL/Horizons is on the order of hundreds of meters, whereas orbital deviations introduced by different ring model strategies range from several to tens of meters.

**Discussion:** The accuracy of Mars orbit determination is influenced by the precision and quantity of multi-source observations, as well as the strategies for ring model construction.

### KEYWORDS

dynamical modeling, main-belt modeling, mars numerical ephemeris, numerical integration methods, small perturbations

## 1 Introduction

The analysis of Mars orbital dynamics, along with the relative motions and mutual gravitational interactions among Solar System bodies, not only illuminates the underlying dynamical principles of celestial mechanics but also provides critical constraints for the inverse modelling of Mars internal structure and physical parameters. In celestial mechanics, the planetary ephemerides are generally classified as analytical and numerical methods. Since the 1960s, with the rapid evolution of deep-space exploration technologies and observing capabilities, the available data have dramatically increased. The classical analytical theories have become inadequate to satisfy the stringent accuracy demands of modern radio-tracking measurements. Numerical methods, by virtue of their flexibility and superior precision, have therefore emerged as the predominant methodology for planetary ephemerides.

At present, several international institutions publish high-precision numerical ephemerides, the DE440 and DE441 ephemerides from the Jet Propulsion Laboratory

(JPL) (Park et al., 2021), the EPM2021 and EPM 2021H series from the Institute of Applied Astronomy (IAA) (Pitjeva et al., 2019; Pitjeva and Pavlov, 2021), the INPOP21a ephemeris by the Institut de Mécanique Céleste et de Calcul des Éphémérides (IMCCE) (Fienga et al., 2021), and the PETREL19 ephemeris (Tian, 2023). These widely used planetary ephemerides differ in their strategies for data selection and the treatment of perturbation models, especially for the Mars ephemeris. DE440/DE441 incorporated the observations from Mars orbiters spanning 2013–2020, including Mars Express (MEX) and Mars Reconnaissance Orbiter (MRO), and further used the Very Long Baseline Interferometry (VLBI) measurements of those orbiters to align the inertial planetary dynamical reference frame precisely with the latest International Celestial Reference Frame (ICRF 3.0). This alignment attains an average precision of approximately 0.2 milliarcseconds. INPOP21a augmented its fit dataset with 2 years of MEX normal points based on its previous product. EPM2021/EPM 2021H incorporated recent optical observations and range measurements from MRO and Mars Odyssey (ODY) for 2014–2017, and to address systematic errors in the MRO and ODY range residuals, they developed the site-specific radio-observatory bias calibration and a DSN station-specific bias correction model (Kuchynka et al., 2012). It is noteworthy that DE440/DE441, INPOP21a, and PETREL19 excluded Mars historical radar range measurements and optical angular observations, instead relying on radiometric range, VLBI, and Very Long Baseline Array (VLBA) observations, while EPM2021 incorporated 403 radar observations during 1965–1995.

The paper is structured as follows. Section 2 introduces the perturbation models and modeling strategies adopted in ephemerides. Section 3 provides a brief overview of the numerical integrators used in major planetary ephemerides, focusing primarily on the quantitative assessment of various perturbation forces on the orbital motion of Mars. Section 4 examines the observation quality, the main-belt asteroid models, and weak perturbations that affect the precision of orbit refinement. Section 5 summarizes the conclusions.

## 2 Mars orbital perturbations

In the Mars orbital numerical integration, the dynamical model comprehensiveness dictates not only the orbit accuracy but also the computational cost and efficiency. To achieve high accuracy and computational efficiency in long-term orbital predictions, the force model must encompass all perturbations that can produce appreciable cumulative effects, while permitting judicious simplification or omission of minor terms depending on the chosen integration interval and target precision. Table 1 summarizes the dynamical ingredients adopted in JPL DE440/DE441, IAA EPM2021/EPM 2021H, IMCCE INPOP21a, and PETREL19.

### 2.1 Principal items

The point mass mutual interactions between the Sun, the eight major planets, Pluto, and the Moon encompass both the classical N-body gravitational perturbations and the post-Newtonian corrections introduced by general relativity. These interactions are calculated using a parameterized post-Newtonian N-body metric (Einstein et al., 1938; Will and Nordtvedt, 1972; Moyer, 2005).

Figure perturbations represent the interaction between extended-body nonspherical gravity fields and point masses and are modeled via spherical harmonic expansions. These include the Sun's quadrupole term ( $J_2$ ) and the contributions of higher-degree harmonics for Earth ( $J_n$  ( $n = 2 \dots 6$ ) and  $\dot{J}_2$ ) and of lunar coefficients  $C_{nm}$  ( $n = 2 \dots 6$ ,  $m = 0 \dots n$ ) acting on the point-mass ensemble comprising the Sun, Moon, Mercury, Venus, Mars, Jupiter, and Saturn. Over a 30-year integration interval, the solar oblateness exerts the dominant figure perturbation, with an effect on Mars' orbit that markedly exceeds those arising from the aspherical figures of Earth and Moon. In addition to the Sun, other celestial bodies are subject to the gravito-magnetic effect of GTR (the Lense-Thirring effect) induced by general relativity (Moyer, 2005; Park et al., 2017; Park et al., 2021).

Tidal effects include the Earth tides raised by the Sun and Moon, and their interactions with the Sun, Moon, Mercury, Venus, Mars, and Jupiter, as well as lunar tides raised by the Earth, interacting with the Sun, Mercury, Venus, Earth, Mars, and Jupiter. For tidal modeling, a five-time-delay model is used for Earth tides and a one-time-delay model for lunar tides (Williams et al., 2013; Folkner et al., 2014; Tian, 2023).

### 2.2 Small asteroids

To construct a high accuracy dynamical model for Mars, the perturbations caused by the Main Belt Asteroids (MBAs) and Kuiper Belt Objects (KBOs) must be incorporated. Current numerical ephemerides adopt different modeling strategies, which affect both the long-term stability of the ephemerides and the short-term precision of orbit determination. Owing to the immense number of asteroids, explicitly accounting for perturbations from hundreds of thousands or even millions of individual asteroids in Solar System dynamics incurs prohibitive algorithmic and temporal complexity. To reconcile accuracy with computational tractability, modern ephemerides typically employ either a discrete point-mass model or hybrid methods combining point-mass representations with ring-like mass distributions.

#### 2.2.1 Main belt

The perturbations induced by MBAs exert the strongest influence on Mars and Jupiter (Fienga et al., 2020; Liu et al., 2022). The DE series and PETREL19 adopt a point-mass model. DE441 and PETREL19 account for perturbations from 343 of the most massive MBAs while neglecting the cumulative perturbation from the remaining main-belt asteroid population. The EPM series enhances the point-mass method by incorporating an ecliptic ring model to represent MBAs that are not modeled individually, and estimates the mass of the residual belt by fitting observations (Pitjeva, 2013; Pitjeva et al., 2019). The early versions of the INPOP series combined point-mass models with a ring model. INPOP06 introduced a static circular ring centered on the Solar System barycenter (Fienga et al., 2008), INPOP08 further refined the model by allowing the ring to co-move with the planets, thereby eliminating center-of-mass drift, but the more recent INPOP19a and INPOP21a considered only 343 MBAs (Fienga et al., 2009; Park et al., 2017; Park et al., 2021).

TABLE 1 Dynamical models considered for the ephemerides.

Dynamical model	DE440/441 (Park et al., 2021)	INPOP21a (Fienga et al., 2021)	EPM2021 (Pitjeva and Pavlov, 2021)	PETREL19 (Tian, 2023)
Point-Mass	✓	✓	✓	✓
Figure Effect	✓	✓	✓	✓
	(Sun, Earth and Moon)	(Sun and Earth)	(Sun, Earth and Moon)	(Sun, Earth and Moon)
Tidal Effect	✓	✓	✓	✓
	(Earth and Moon)	(Earth)	(Earth and Moon)	(Earth and Moon)
Lense-Thirring	✓	✓	✓	×
Main Asteroid Belt	✓	✓	✓	✓
	(343 Asteroids)	(277 Asteroids+3 Rings (2.2, 2.74, 3.0 AU))	(343 Asteroids)	(343 Asteroids)
Kuiper Belt	✓	✓	✓	×
	(30 Asteroids+1 Ring (44 AU))	(31 Asteroids+3 Rings (39.4, 44.0, 48.7 AU))	(500 Asteroids)	

The one-ring model proposed by Kuchynka et al. (2010), Kuchynka et al. (2010) and the six-ring model proposed by Liu et al. (2023), Liu et al. (2023) replace main-belt asteroids that are not individually modeled or are unknown with ring-shaped mass distributions. This approach balances universality, computational efficiency, and high-precision requirements (Liu, 2021; Liu et al., 2022; Liu et al., 2023). The parameters employed for the typical point-mass model, one-ring model, and six-ring model are presented in Table 2.

## 2.2.2 Kuiper belt

The Kuiper belt comprises millions of small bodies predominantly distributed in an annular region between approximately 39.4 and 47.8 AU, and its total mass exceeds that of the main asteroid belt (Pitjeva and Pitjev, 2018a). KBOs are conventionally classified into two dynamical populations according to their orbital characteristics, classical objects and resonant objects. Classical KBOs form the numerically dominant component. They occupy the 40–50 AU region, exhibit near-circular, low-eccentricity orbits, and constitute the principal reservoir of the belt. Resonant KBOs are in mean-motion orbital resonance with Neptune.

Planetary ephemerides employ a variety of strategies to model the Kuiper Belt. DE440 and DE441 select 30 individual KBOs and model the remaining belt as an annular perturbation represented by 36 equal-mass point masses uniformly distributed at 44 AU. INPOP19a estimates the mass of an outer-Neptune annulus located between the 2:1 and 3:2 mean-motion resonances and introduced three circular ring models at 39.4, 44.0, and 47.5 AU. From an initial set of 2,225 KBOs extracted from the Astorb database (semi-major axes 39.3–47.6 AU), INPOP21a randomly selected 500 objects and integrated them as individual point masses. Their orbits were directly taken from the Astorb database, providing a more realistic representation of the eccentricity and semi-major-axis distributions. However, the orbits were assumed to lie in the ecliptic plane with zero inclination. Equal masses were assigned to the 500 selected objects. A full fit was then performed for each random sample,

estimating their total mass together with the standard planetary ephemeris parameters. Results were very similar across different random selections, and one sample was therefore arbitrarily retained for the subsequent analysis (Pitjeva, 2010; Fienga et al., 2021). The EPM series has incorporated Kuiper-belt effects since EPM2008 via a combined point-mass and ring model, and estimates the belt mass by Cassini tracking data as well. The dynamical estimate of the Kuiper belt mass within the EPM series ephemeris is presented in Table 3.

## 3 Numerical integration framework

The impact of various perturbation forces on the evolution of Mars orbital motion is systematically evaluated using the Mars dynamical model assembled in Section 2. The dynamical model includes the following components: (A) point-mass gravitational interactions among the Sun, planets, Pluto and the Moon; (B) perturbations from 343 MBAs; (C) perturbations from 30 KBOs; (D) an annular Kuiper belt representation implemented as 36 equal-mass point masses uniformly distributed at 44 AU; (E) the solar oblateness ( $J_2$ ); and (F) the Lense-Thirring effect.

### 3.1 Integration methods

Numerical integration methods commonly employed in planetary ephemeris calculations include single-step methods, such as Bulirsch-Stoer (BS) and Runge-Kutta-Fehlberg (RKF), multistep methods exemplified by Adams-Bashforth-Moulton (ABM), and implicit methods based on Gauss-Radau. These integrators trade off stability, convergence, and local/global error control, step-size adaptivity strategies, and computational efficiency in different ways. The JPL DE series employs a variable-step, variable-order Adams method. INPOP adopts a classical 12th-order Adams PECE integrator. The EPM ephemerides utilise proprietary Ephemeris Research in Astronomy (ERA) software to implement multiple integration methods, including Everhart, Gauss-Everhart, and ABMD variants derived from multi-step ABM strategies (Aksim

TABLE 2 Comparison of asteroid belt models in different ephemerides.

Ephemeris	Model	Point-mass/ Ring	Ring radius (AU)	GM (km <sup>3</sup> /s <sup>2</sup> )
DE441 (Park et al., 2021)	Point-mass	343 <sup>a</sup>	–	170.5321
EPM 2014 (Pitjeva and Pitjev, 2015)	Point-mass	301	–	148.4521
	Two-ring	R1	2.060	14.0543
		R2	3.270	
EPM 2017 (Pitjeva and Pitjev, 2018b)	Point-mass	301	–	153.0307
	Three-ring	R1	2.060	6.7284
		R2	2.670	
		R3	3.270	
EPM 2021 (Pitjeva et al., 2019)	Point-mass	277	–	160.0972
	Three-ring	R1	2.200	4.5553
		R2	2.740	
		R3	3.000	
INPOP-related (Kuchynka et al., 2010)	One-ring	R1	2.784	2.1157
INPOP-related (Liu et al., 2022; Liu et al., 2023)	Six-ring	R1	2.784	11.2549
		R2	2.383	
		R3	2.316	
		R4	3.165	
		R5	2.601	
		R6	3.098	

<sup>a</sup>The total number of main-belt asteroids modeled as point masses is 343.

TABLE 3 Dynamical mass estimates for the Kuiper belt.

Ephemerides	Mass of ring	Total mass
EPM2008 (Pitjeva, 2008, Pitjeva, 2010)	$1.66 \times 10^{-2} m_{\oplus}$	$2.58 \times 10^{-2} m_{\oplus}$
EPM2011 (Pitjeva, 2013)	$(1.67 \pm 0.83) \times 10^{-2} m_{\oplus}$	$2.63 \times 10^{-2} m_{\oplus}$
EPM2013 (Pitjeva and Pitjev, 2014)	$(1.08 \pm 0.59) \times 10^{-2} m_{\oplus}$	$2.63 \times 10^{-2} m_{\oplus}$
EPM2016 (Pitjeva and Pitjev, 2016)	$(1.45 \pm 0.41) \times 10^{-2} m_{\oplus}$	$(2.28 \pm 0.46) \times 10^{-2} m_{\oplus}$
EPM2017 (Pitjeva and Pitjev, 2018a; Pitjeva and Pitjev, 2018b)	$(1.108 \pm 0.25) \times 10^{-2} m_{\oplus}$	$(1.97 \pm 0.35) \times 10^{-2} m_{\oplus}$
EPM2021 (Pitjeva and Pavlov, 2021)	$(1.60 \pm 0.10) \times 10^{-2} m_{\oplus}$	$(2.34 \pm 0.20) \times 10^{-2} m_{\oplus}$

and Pavlov, 2020). PETREL19 uses a fixed-order, fixed-step Adams-Cowell PECE implementation.

The BS integrator is selected for the orbital integration. Initial epochs and orbital states are obtained from the JPL/Horizons system. The integration period is set to 100 years (1974–2074) with a step size of 1 day. The discrepancy between the self-integrating orbit and the JPL/Horizons DE441 ephemeris is plotted in Figure 1.

As shown in Figure 1, the maximum orbital differences relative to DE441 over the century-long integration is approximately 500 m, with positional RMS values falling within the range of 10–100 m. The Fast Fourier Transform (FFT) spectral analysis presented in Figure 1 reveals a dominant spectral peak at 688.87 days. This periodicity aligns closely with the Mars orbital period (687 days), distinct from the Earth-Mars synodic period (780 days). Furthermore, the notable absence of significant high-frequency noise in the spectrum effectively rules out numerical artifacts associated with the integrator step size.

### 3.2 Perturbing effects

To evaluate the influence of individual perturbations on the evolution of Mars orbital motion, numerical integrations were performed using the BS over the period from 1995 to 2026, with a fixed 1-day step. Initial orbital states, body GM values, and the solar  $J_2$  parameter were adopted from the DE440/DE441 ephemerides. Planetary and small-body ephemerides were obtained from DE441 and its companion small-body catalog SB441-N373. Figure 2 illustrates the effects of planetary N-body perturbations, small-body populations, and other perturbing forces on the Martian orbit.

Figure 2 illustrates that, over a 30-year timespan, solar gravitational perturbation significantly outweighs all other forces, while the combined perturbations from the planets, Pluto, and the Moon result in a maximum deviation on the order of  $10^6$  km. Within

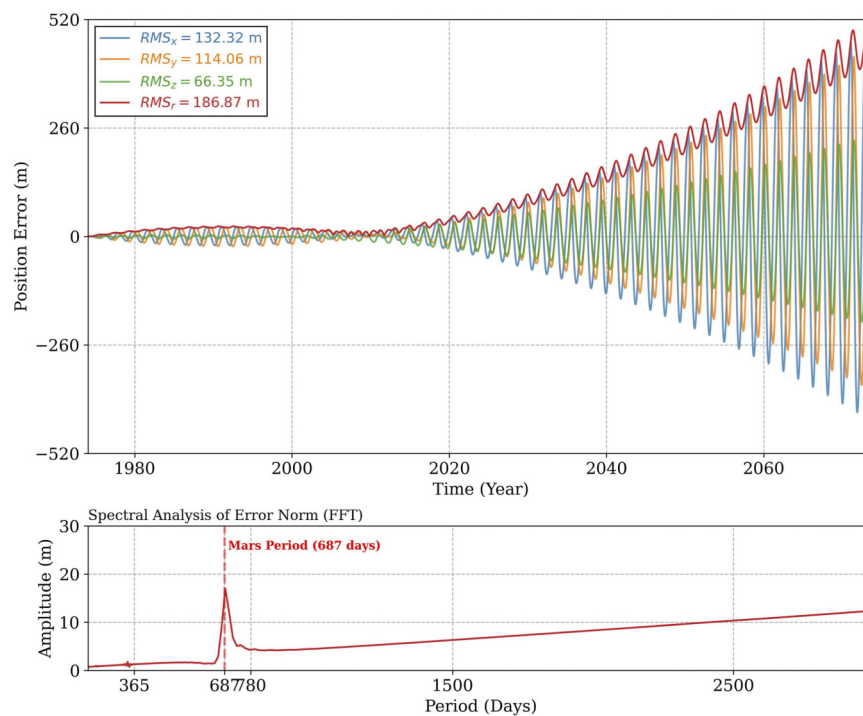


FIGURE 1 Mars orbits differences between self-integrating and DE441 with spectral analysis (FFT).

the post-Newtonian corrections, the solar contribution remains dominant, with effects on the order of  $10^2$  km. Solar oblateness ( $J_2$ ) and the LT effect induce smaller deviations of approximately  $10^{-1}$  km and  $10^{-2}$  km, respectively. While these two effects are minor compared to the dominant perturbations, their influence becomes progressively more pronounced as the integration time increases.

Higher-degree aspherical gravitational terms of Earth and Moon, along with tidal dissipation, accumulate insignificantly over decadal timescales, remaining well below the influence of solar oblateness and the LT effect. As a result, these small perturbations can be selectively omitted to enhance computational efficiency in routine decadal orbital integrations. However, small perturbations should be incorporated selectively when modeling orbital evolution over centennial to millennial timescales.

The choice of model for the main asteroid belt leads to varying effects on the orbital evolution of Mars. Over a 30-year interval, a discrete point-mass model of 343 massive MBAs, which account for the majority of the main belt's mass, dominates the small-body induced deviation of Mars motion, with an impact on the order of  $10^1$  km. In contrast, the one-ring and six-ring models result in perturbations on the order of  $10^{-2}$  km, which are smaller than the point-mass model but nevertheless non-negligible.

Kuiper belt perturbations are represented by the point-mass plus ring model, consistent with the DE440/DE441 ephemerides. As shown in Figure 2, over the same 30-year interval, the ensemble of 30 large KBOs and the annular ring representing the unmodeled residual KBO population each induce Martian positional deviations of  $10^{-2}$  km. These perturbations are substantially smaller than those generated by the main asteroid belt.

The point-mass model for the Kuiper belt and the ring model representing the unmodeled KBO population, which accounts for approximately 60% of the total mass of the Kuiper belt, exert comparable effects on Mars orbit. Therefore, for long-term, high-precision numerical integrations and orbital predictions, a combined point-mass and ring model is recommended. This strategy balances computational feasibility and efficiency while more comprehensively reflecting the perturbative effects of Kuiper belt objects.

## 4 Mars orbit solution

In the construction of Mars ephemerides, variations in the precision and temporal coverage of multi-source observational datasets significantly impact orbit determination results. Furthermore, discrepancies in the formulation of perturbation models, including model structure and parameter selection, lead to differences in Mars orbital calculations. Additionally, certain weak perturbations, though often excluded, may accumulate and cause non-negligible biases in high-precision orbit determination. Therefore, further analysis is conducted on the impact of variations in the quality of multi-source observations, different perturbation models for the same gravitational force, and the weak gravitational forces not yet incorporated into existing models on Mars orbital determination. The orbit determination period spans from 1974 to 2074 (100 years), with initial states for Mars sourced from the JPL/Horizons system at the epoch 2005-03-08 12:00:00.0 TDB.

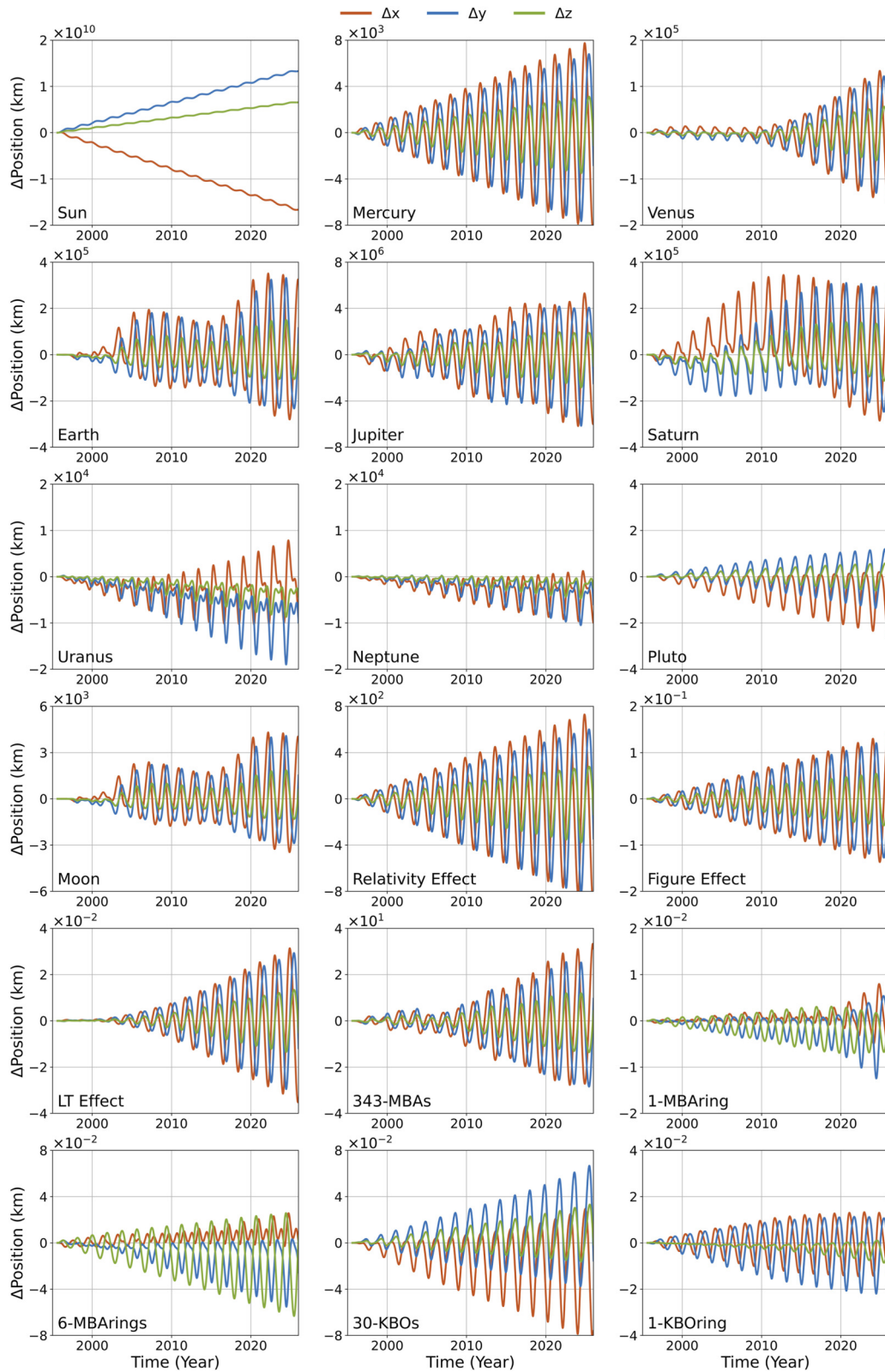


FIGURE 2 Effects of typical perturbing forces on the orbit of Mars.

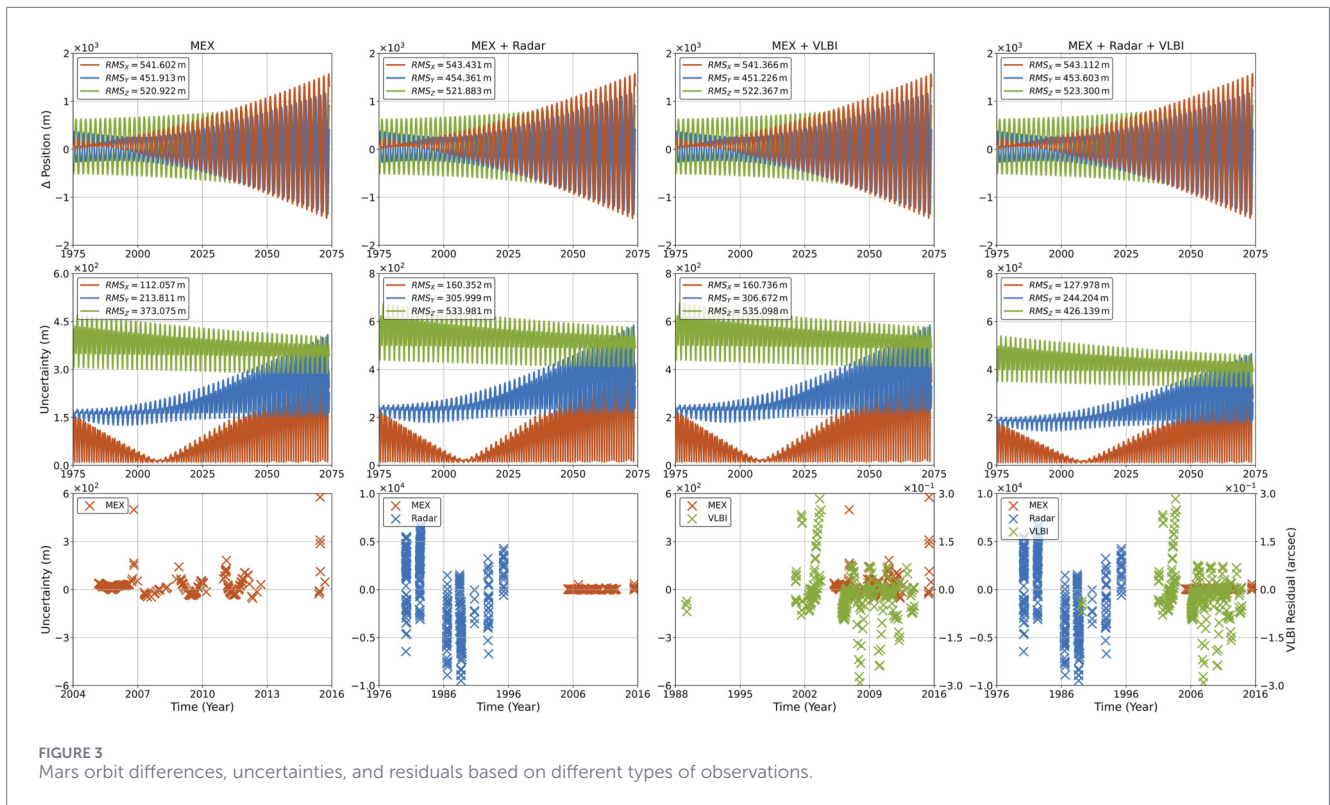


FIGURE 3 Mars orbit differences, uncertainties, and residuals based on different types of observations.

### 4.1 Observations

Three types of observations are selected for orbit solving of Mars and evaluated the impact of differences in accuracy and spatiotemporal coverage of observations. The observations are obtained from the APDB and Planetary Observational Data, and include radar range from 1980 to 1995 (381 observations), ranging data of Mars Express (MEX) from 2006 to 2016 (272 observations), and VLBI measurements from 1989 to 2013 (194 observations). A weighting scheme based on the average precision of observations is implemented. The standard deviations are assigned as 1,000 m for ground-based radar ranging, 0.3 mas for VLBI, and 2 m for MEX ranging. The solving orbit is compared with the JPL/Horizons DE441, shown in Figure 3.

Figure 3 demonstrates the impact of different observations on orbit solutions. Incorporating VLBI into the orbit determination leads to a reduction in positional differences. However, when both ground-based radar ranging and VLBI are included, the positional differences exhibit a slight increase. Nevertheless, by employing different data combinations and assigning weights based on average measurement precision, the position difference RMS is on the order of hundred-meter level. The precision, quantity, and temporal distribution of observations are critical factors for achieving high-accuracy Mars orbit determination.

### 4.2 Belt modeling

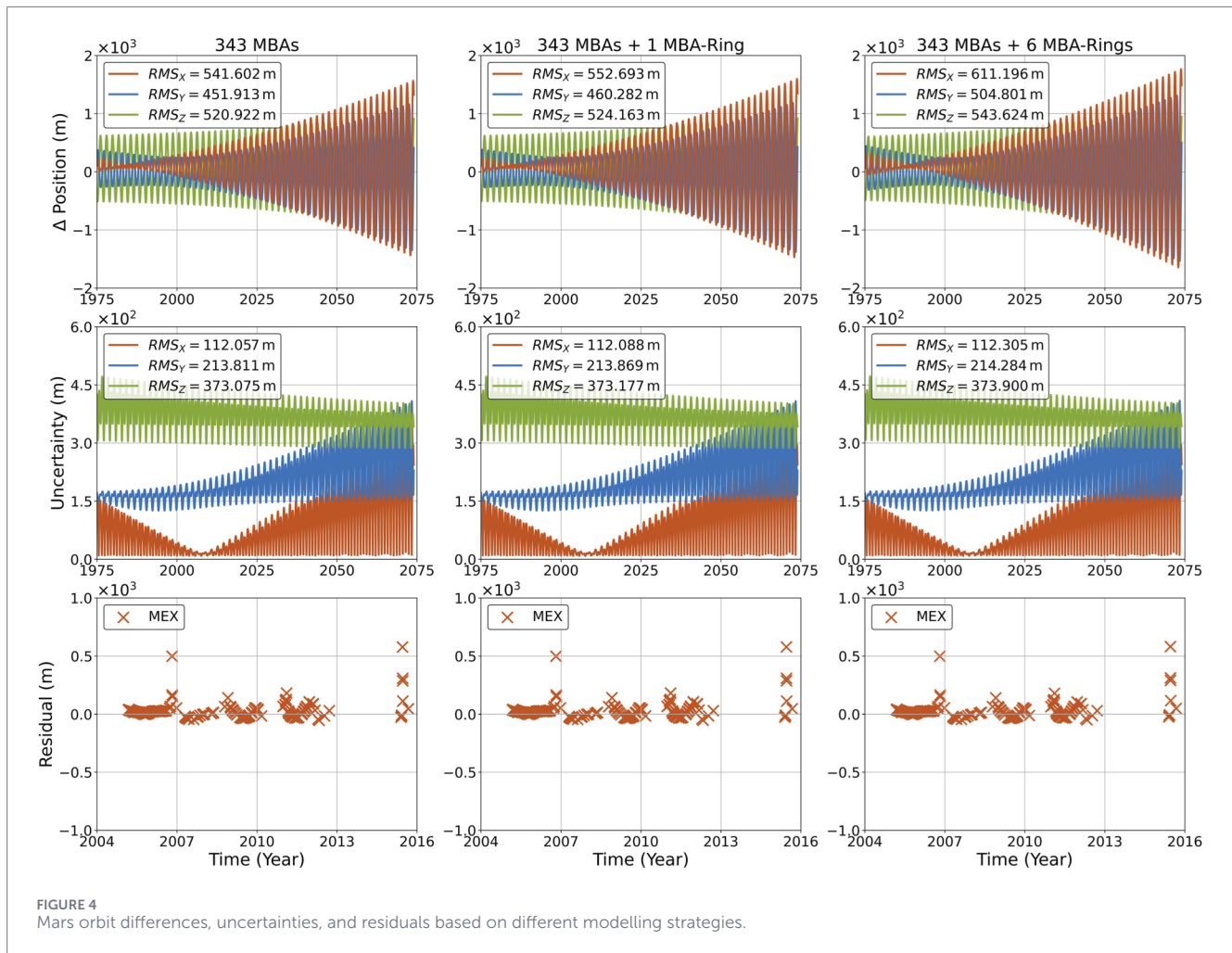
Main asteroid-belt perturbations significantly affect the accuracy of Martian dynamical parameter estimation. Section 3 introduced three representative models for the main belt, the point-mass model representing large asteroids, the one-ring model, and

the six-ring model used to approximate the unmodeled MBAs. The point-mass model for 343 large asteroids, which accounts for over 90% of the main asteroid belt mass, can induce perturbations on the order of kilometers, whereas the ring models, representing unmodeled asteroids, produce effects on the order of meters. As integration time increases, the cumulative effects of the ring models become more pronounced, exerting a significant impact on Mars orbit evolution. Thus, different modeling strategies for the main belt are investigated to assess their influence on Mars orbit.

The parameters of the point-mass and annular models used in this study, including ring radii, total GM, and other relevant characteristics, are provided in Table 2. The point-mass model for the 343 MBAs follows DE441, while the parameters of the one-ring and six-ring models can refer to Liu et al. (2023), Liu et al. (2023). To assess the impact of different modeling strategies, the orbit solving was performed using only MEX ranging spanning 2006-2016, and ring model parameters were fixed. The difference between our results and the JPL/Horizons DE441 is shown in Figure 4.

From Figures 2, 4, different modelling strategies for the ring-belt model exert varying effects on the final orbital determination results and the positional differences between the models, ranging from a few meters to several tens of meters.

As detailed in Section 3.2, the influence of Earth and lunar figure perturbations, as well as tidal effects, on mid- to short-term Martian orbit integrations is generally below detectable levels. However, during the orbit determination process, Figure perturbations of Earth exert a minor influence, and in ultra-long integrations and scenarios, these subtle perturbations may lead to a non-negligible difference in the final orbit evolution.



## 5 Conclusion

This paper provides a comparative analysis of the dynamical models used in recent Mars ephemerides based on DE441, EPM 2021, INPOP21a, and PETREL19. The different ephemerides place varying emphasis on model construction, parameter determination, and the treatment of perturbative effects, with notable discrepancies in the selection and modeling of main-belt asteroids and Kuiper belt objects.

In Mars orbit, the solar gravitational influence overwhelmingly dominates that of other celestial bodies. The gravitational perturbations from the seven major planets, the Moon, and Pluto are the next most influential, with their effects on orbit calculations being of the order of approximately  $10^6$  km. Perturbations from small bodies, such as those in the main asteroid belt and Kuiper belt, as well as the solar oblateness and the LT effect, produce relatively small positional deviations, though they must be considered in long-term orbital integrations. The effects produced by different perturbation models applied to the main asteroid belt and the Kuiper belt also differ. The acceleration caused by higher-order non-spherical perturbations and tidal dissipation, both from Earth and the Moon, is extremely weak, and its cumulative impact on the orbit is much less significant than that of subtle perturbations

like the LT effect, which are difficult to detect. These effects may be neglected in medium- to short-term orbital integrations.

Mars orbit solving is highly sensitive to the precision, quantity, and temporal distribution of multi-source observations. When MEX ranging, ground-based radar, and VLBI data are combined for Mars orbit determination, with weights assigned based on the average precision of each dataset, the positional differences RMS remain at the hundred-meter level. Differences in ring model construction strategies impact orbital determination accuracy. When employing different models for small bodies in the main belt, positional deviations from JPL/Horizons DE441 remain within the order of hundreds of meters. Over a centennial timescale, discrepancies between the point-mass model and ring models are on the order of a few to several tens of meters. Moreover, the weak perturbations can also affect the precision of Mars orbit solving.

## Data availability statement

The original contributions presented in the study are included in the article/supplementary material, further inquiries can be directed to the corresponding authors.

## Author contributions

SF: Writing – original draft. YH: Writing – review and editing. SL: Writing – review and editing, Writing – original draft. KT: Writing – review and editing. JY: Writing – review and editing.

## Funding

The author(s) declared that financial support was not received for this work and/or its publication.

## Conflict of interest

The author(s) declared that this work was conducted in the absence of any commercial or financial relationships that could be construed as a potential conflict of interest.

## References

- Aksim, D., and Pavlov, D. (2020). On the extension of adams–bashforth–moulton methods for numerical integration of delay differential equations and application to the moon's orbit. *Math. Comput. Sci.* 14, 103–109. doi:10.1007/s11786-019-00447-y
- Einstein, A., Infeld, L., and Hoffmann, B. (1938). The gravitational equations and the problem of motion. *Ann. Math.* 39, 65–100. doi:10.2307/1968714
- Fienga, A., Manche, H., Laskar, J., and Gastineau, M. (2008). INPOP06: a new numerical planetary ephemeris. *Astron. Astrophys.* 477, 315–327. doi:10.1051/0004-6361/20066607
- Fienga, A., Laskar, J., Morley, T., Manche, H., Kuchynka, P., Le Poncin-Lafitte, C., et al. (2009). INPOP08, a 4-D planetary ephemeris: from asteroid and time-scale computations to ESA Mars express and Venus express contributions. *Astron. Astrophys.* 507, 1675–1686. doi:10.1051/0004-6361/200911755
- Fienga, A., Viswanathan, V., Deram, P., Di Ruscio, A., Bernus, L., Laskar, J., et al. (2020). INPOP new release: INPOP19a. *Astron. Earth rotat., Ref.* 293–297.
- Fienga, A., Deram, P., Di Ruscio, A., Viswanathan, V., Camargo, J. I. B., Bernus, L., et al. (2021). *INPOP21a planetary ephemerides. Scientific and technical note S110*. Paris: Institut de mécanique céleste et de calcul des éphémérides (IMCCE).
- Folkner, W. M., Williams, J. G., Boggs, D. H., Park, R. S., and Kuchynka, P. (2014). The planetary and lunar ephemerides DE430 and DE431. *Ipn. Prog. Rep.* 196, 42–196.
- Kuchynka, P., Laskar, J., Fienga, A., and Manche, H. (2010). A ring as a model of the main belt in planetary ephemerides. *Astron. Astrophys.* 514, A96. doi:10.1051/0004-6361/200913346
- Kuchynka, P., Folkner, W. M., and Konopliv, A. S. (2012). Station-specific errors in Mars ranging measurements. *Ipn. Prog. Rep.* 42, 190.
- Liu, S. (2021). *Scientific applications of radio tracking data from deep space probes (in Chinese)*. Wuhan: Wuhan University. Ph.D. thesis.
- Liu, S., Fienga, A., and Yan, J. (2022). A ring model of the main asteroid belt for planetary ephemerides. *Icarus* 376, 114845. doi:10.1016/j.icarus.2021.114845
- Liu, S., Wu, Z., Cao, J., Yan, J., and Li, X. (2023). Impact analysis of the main asteroid belt on the long-term dynamics of Mars orbit. *Sci. Sin. Phys. Mech. Astron.* 53, 229511. doi:10.1360/sspma-2022-0119
- Moyer, T. D. (2005). *Formulation for observed and computed values of deep space network data types for navigation*. John Wiley and Sons.
- Park, R. S., Folkner, W. M., Konopliv, A. S., Williams, J. G., Smith, D. E., and Zuber, M. T. (2017). Precession of mercury's perihelion from ranging to the MESSENGER spacecraft. *Astron. J.* 153, 121. doi:10.3847/1538-3881/aa5be2

## Generative AI statement

The author(s) declared that generative AI was not used in the creation of this manuscript.

Any alternative text (alt text) provided alongside figures in this article has been generated by Frontiers with the support of artificial intelligence and reasonable efforts have been made to ensure accuracy, including review by the authors wherever possible. If you identify any issues, please contact us.

## Publisher's note

All claims expressed in this article are solely those of the authors and do not necessarily represent those of their affiliated organizations, or those of the publisher, the editors and the reviewers. Any product that may be evaluated in this article, or claim that may be made by its manufacturer, is not guaranteed or endorsed by the publisher.

- Park, R. S., Folkner, W. M., Williams, J. G., and Boggs, D. H. (2021). The JPL planetary and lunar ephemerides DE440 and DE441. *Astron. J.* 161, 105. doi:10.3847/1538-3881/abd414
- Pitjeva, E. V. (2008). Ephemerides EPM2008: the updated model, constants, data. *Proc. Journées Syst. Réf. Spatio-Temporels X Lohrmann-Kolloquium*, 22–24.
- Pitjeva, E. V. (2010). "Influence of asteroids and Trans-Neptunian objects on the motion of major planets and masses of the asteroid main belt and the TNO ring," in *Proc. Int. Conf. asteroid–comet hazard*, 237–241.
- Pitjeva, E. V. (2013). Updated IAA RAS planetary ephemerides-EPM2011 and their use in scientific research. *Sol. Syst. Res.* 47, 386–402. doi:10.1134/s0038094613040059
- Pitjeva, E. V., and Pavlov, D. A. (2021). *EPM2021 and EPM2021H*. St. Petersburg: Institute of Applied Astronomy RAS (IAA RAS). Technical report.
- Pitjeva, E. V., and Pitjev, N. P. (2014). Development of planetary ephemerides EPM and their applications. *Celest. Mech. Dyn. Astron.* 119, 237–256. doi:10.1007/s10569-014-9569-0
- Pitjeva, E. V., and Pitjev, N. P. (2015). Masses of asteroids and total mass of the main asteroid belt. *Proc. Int. Astron. Union* 10, 212–217. doi:10.1017/s1743921315008388
- Pitjeva, E. V., and Pitjev, N. H. (2016). "Asteroids: new observations, new models," in *Proceedings of the IAU symposium no. 318 on asteroids: new observations, new models*. Editors S. Chesley, A. Morbidelli, R. Jedicke, and D. Farnocchia (Cambridge University Press), 212.
- Pitjeva, E. V., and Pitjev, N. P. (2018a). Mass of the kuiper belt. *Celest. Mech. Dyn. Astron.* 130, 57. doi:10.1007/s10569-018-9853-5
- Pitjeva, E. V., and Pitjev, N. P. (2018b). Masses of the main asteroid belt and the kuiper belt from the motions of planets and spacecraft. *Astron. Lett.* 44, 554–566. doi:10.1134/s1063773718090050
- Pitjeva, E., Pavlov, D., Aksim, D., and Kan, M. (2019). Planetary and lunar ephemeris EPM2021 and its significance for solar system research. *Proc. Int. Astron. Union* 15, 220–225. doi:10.1017/s1743921321001447
- Tian, W. (2023). PETREL19: a new numerical solution of planetary and lunar ephemeris. *Celest. Mech. Dyn. Astron.* 135, 38. doi:10.1007/s10569-023-10151-6
- Will, C. M., and Nordtvedt, K. J. (1972). Conservation laws and preferred frames in relativistic gravity. i. preferred-frame theories and an extended PPN formalism. *Astrophys. J.* 177 (3), 757–774. doi:10.1086/151754
- Williams, J. G., Boggs, D. H., and Folkner, W. M. (2013). DE430 lunar orbit, physical librations and surface coordinates. *JPL Interoffice Memo.* 19, 1–19.